Talin2-mediated traction force drives matrix degradation and cell invasion

Lei Qi[1,2*], Naser Jafari[1,2 *], Xiang Li[1*], Zaozao Chen[3], Liqing Li[1], Vesa P. Hytönen[4], Benjamin T. Goult[5], Chang-Guo Zhan[6], and Cai Huang[1,2,7]

[1]Markey Cancer Center, University of Kentucky, Lexington, KY 40506; [2]Veterans Affairs Medical Center, Lexington, KY 40502; [3]Department of Cell Biology & Physiology, University of North Carolina at Chapel Hill, Chapel Hill, NC 27599; [4]BioMediTech, University of Tampere, 33520 Tampere, Finland and Fimlab Laboratories, 33520 Tampere, Finland; [5]School of Biosciences, University of Kent, Canterbury, Kent CT2 7NJ, UK; [6]Molecular Modeling and Biopharmaceutical Center, College of Pharmacy, University of Kentucky, Lexington, KY 40506; [7]Department of Pharmacology and nutritional sciences, University of Kentucky, Lexington, KY 40506

*These authors contribute equally

Author for correspondence

Cai Huang

Markey Cancer Center and

Department of Pharmacology and Nutritional Sciences

University of Kentucky

BBSRB Room B359

741 South Limestone

Lexington, KY 40506-0509

Tel:(859)3239577

Email: cai-huang@uky.edu

Running title: Talin2 in traction force and invasion

Key words: talin1, talin2, traction force, focal adhesions, cell invasion

Summary statement

Talin2, previously presumed to function redundantly with talin1, is indispensable for the generation of traction force, which in turn mediates matrix degradation and cell invasion.

Abstract

Talin binds β-integrin tails to activate integrins, regulating cell migration, invasion and metastasis. There are two talin genes, *Tln1* and *Tln2*, encoding talin1 and talin2, respectively. While talin1 regulates focal adhesion dynamics, cell migration and invasion, the biological function of talin2 is not clear and indeed talin2 has been presumed to function redundantly with talin1. Here we show that talin2 has a much stronger binding to β-integrin tails than talin1. Substitution of talin2 Ser339 with Cys significantly decreased its binding to β1-integrin tails to a level comparable to that of talin1. Talin2 localizes at invadopodia and is indispensable for traction force and invadopodium-mediated matrix degradation. Ablation of talin2 suppressed traction force generation and invadopodia, which were restored by re-expressing talin2 but not talin1. Furthermore, re-expression of WT talin2 (but not talin2^{S339C}) in talin2-depleted cells rescued traction force development and invadopodia. These results suggest that a strong interaction of talin2 with integrins is required to generate traction, which in turn drives invadopodium-mediated matrix degradation, key to cancer cell invasion.

Introduction

Talin activates integrin and plays a pivotal role in cell migration, invasion and cancer metastasis (Desiniotis and Kyprianou, 2011; Huang et al., 2009; Jin et al., 2015; Tadokoro et al., 2003). Talin contains an amino-terminal globular head domain and a carboxy-terminal rod domain (Goult et al., 2013; Nuckolls et al., 1990). The talin head domain contains a FERM domain, and is responsible for the binding of talin to β-integrin tails (Calderwood et al., 1999). The rod domain has several vinculin-binding sites, and two actin-binding sites (Atherton et al., 2015; Gingras et al., 2005; Hemmings et al., 1996). The binding of talin to β-integrin tails is essential for integrin activation (Calderwood et al., 1999; Tadokoro et al., 2003), which in turn regulates focal adhesion (FA) dynamics and invadopodium formation (Bate et al., 2012; Beaty et al., 2014; Franco et al., 2004; Nayal et al., 2004), key steps in cell migration and invasion (Beaty and Condeelis, 2014; Saykali and El-Sibai, 2014; Webb et al., 2002; Wehrle-Haller, 2012). Talin also mediates calpain-induced FA disassembly (Bate et al., 2012; Franco et al., 2004). Talin1 phosphorylation by Cdk5 regulates FA dynamics, integrin activation, cell migration, invasion and metastasis (Huang et al., 2009; Jin et al., 2015). Talin interacts with PIPKIγ, which produces PIP_2 to regulate FA dynamics, cell migration and invasion (Chen et al., 2014; Di Paolo et al., 2002; Li et al., 2013; Ling et al., 2002; Wu et al., 2011). It recruits the moesin-NHE1 complex to modulate pH at invadopodia, consequently governing invadopodium stability and matrix degradation (Beaty et al., 2014). It is also required for the initial generation of mechanical force (Giannone et al., 2003; Zhang et al., 2008).

There are two talin genes, *Tln1* and *Tln2*, encoding talin1 and talin2, respectively. Talin1 has been well studied, while the biological function of talin2 is less clear. It has been shown that talin2 regulates focal adhesion assembly and focal adhesion kinase (FAK) signaling in the absence of talin1 (Zhang et al., 2008). Talin2 is usually localized at large FAs and fibrillar

adhesions, whereas talin1 is usually found at smaller FAs in the peripheral region (Praekelt et al., 2012; Senetar et al., 2007). Trastuzumab, a HER2-targeting antibody drug for cancer therapy, inhibits cell migration and invasion through down-regulating talin2 (Le et al., 2012). Nevertheless, it has been reported that depletion of talin2 does not influence β1-integrin activation (Jin et al., 2015). Thus, it had been presumed that talin2 functions redundantly with talin1.

In the present study, we demonstrate that talin2 functions distinctly from talin1 as a regulator of cell invasion. We show that talin2 has a stronger interaction with β-integrin tails than talin1, and that it co-localizes with invadopodia, regulates traction force generation and invadopodium-mediated matrix degradation. Furthermore, the strong interaction of talin2 with β-integrin tails is essential for the development of strong traction and invadopodia, as substitution of S339 with Cys in the talin2 head domain compromises binding to β-integrin tails, and inhibits traction force and invadopodium-mediated matrix degradation. Recently, a disease causing missense variant, S339L, of the Tln2 gene was identified as the cause of fifth finger camptodactyly, a digit deformity in humans (Deng et al., 2016), which occurred in the presence of talin1, further highlighting distinct roles of talin1 and talin2 in development. This also demonstrates the physiological relevance of S339 in talin2 function and the requirement for a robust talin2:integrin linkage for normal development. Thus, interaction of talin2 with integrins is required for traction force generation, which in turn drives invadopodium-mediated matrix degradation, and ultimately, cancer cell invasion.

Results

Talin2 binds β-integrin tails stronger than talin1

To learn whether talin1 and talin2 have any difference in binding to β-integrin tails, CHO-K1 cells were transfected with EGFP-talin head constructs: EGFP-talin1$_{1-433}$, -talin1$_{1-446}$ or –talin2$_{1-}$

$_{449}$, and binding to integrin tails was determined by GST-β integrin tail pull-down assays, using GST as a control. The interaction of talin2$_{1-449}$ with β1A-integrin tail was more efficient than that of either talin1$_{1-433}$ or talin1$_{1-446}$ (**Fig. 1A**). Similar results were observed with the binding of β3A- and β1D-integrin tails (**Fig. S1A**). Deletion of the carboxyl terminus of the FERM domain enhanced the binding of talin2$_{1-449}$ to β1A tails (**Fig. 1B**), but reduced the binding of talin1$_{1-446}$ (**Fig. 1C**). The difference between talin1 and talin2 in integrin binding was not caused by other associated proteins in the cell lysates, because purified His-tagged talin2$_{1-449}$ binding to β1A-integrin tail was also stronger than purified talin1$_{1-443}$ and talin1$_{1-446}$ (**Fig. 1D**). Thus, the talin2 head domain (TH2) has a much higher affinity than talin1 head domain (TH1) for β-integrin tails.

Talin1 C336 and talin2 S339 contribute to the isoform specific affinity differences

To identify why talin2 binding to integrins is stronger than talin1, we aligned the sequences of talin1 and talin2 around the integrin-binding site in F3. There are several residues that are different between the integrin-binding sequences of talin1 and talin2 (**Fig. 1E**). Substitution of Cys336 of talin1 with Ser enhanced the binding of talin1 to β1A tail to an extent comparable to that of talin2 (**Fig. 1F**), whereas substitution of Ser339 on talin2 with Cys significantly attenuated its binding (**Fig. 1G**). Substitution of Cys336 on talin1 with other residues dramatically changed its binding to β1A tail (**Fig. S1B**), while mutation at several other mismatching residues had no effect on the ability of talin1 binding to integrin tails (data not shown). The recent finding that mutation of Ser339 to Leucine in talin2 has a disease causing phenotype in humans, giving rise to the pathology, fifth finger camptodactyly, highlights the physiological importance of this residue. Indeed, a S339L mutant has a similar effect on integrin binding (**Fig. 1H**). Similar results were observed in pull-down assays using purified His-tagged Tln1$_{1-446}$, Tln2$_{1-449}$ and mutants (**Fig. 1I**). These data indicate that Ser339 plays a significant role in the high integrin binding ability of talin2.

Talin2 is essential for the assembly of large, stable FAs and traction force generation

To ascertain whether talin2 is different from talin1 in regulating FAs, we used CRISPR/Cas9 to knockout talin1 or talin2 from U2 OS cells. Ablation of talin isoforms was achieved by infecting the cells with lentiviruses that express Cas9 and talin1 or talin2 gRNAs (**Fig. 2A**). The talin1- or talin2-null cells were plated on fibronectin and stained for zyxin and either talin1 or talin2, using cells expressing empty LentiCRISPR v2 vector as a control. Ablation of either talin1 or talin2 inhibited the assembly of small FAs (<7 μm^2), as determined by Zyxin staining **(Fig. 2B&C).** However, ablation of talin1 did not influence large FAs (>10 μm^2), whereas talin2 KO significantly diminished the formation of large FAs (**Fig. 2C**, bottom panel). Similar results were observed in cells where talin1- or talin2 were depleted using shRNAs (**Fig. S2A, B&C**). In the central regions (>5 μm from edges) of U2 OS cells, large spots of talin2 were more visible than those of talin1 **(Fig. 2D)**. Likewise, in MDA-MB-231 and MDA-MB-435S cancer cells, talin1 was usually found in smaller FAs, whereas talin2 formed larger FAs **(Fig. S2D&E)**. However, although ablation of talin1 also suppressed the assembly of FAK to small FAs (<7 μm^2), ablation of talin2 had little effect on FAK localization **(Fig. 2E&F).** These results suggest that talin2 is mainly responsible for large, stable FA assembly, while talin1 mediates smaller FA formation.

To compare the roles of talin1 and talin2 in traction force generation, talin1- or talin2-ablated U2 OS cells were plated on fibronectin-conjugated polyacrylamide gels containing Red FluoSpheres, using cells carrying empty CRISPR vector as a control. Traction force was measured using a Nikon A1 confocal microscope equipped with a CO2 incubator system, and analyzed using the method of Butler et al. (Butler et al., 2002). Either talin1 or talin2 knockout (KO) significantly inhibited the traction force (**Fig. 3A&C**). Talin1 KO also significantly depressed the cell spreading on the polyacrylamide gel, whereas talin2 KO had only marginal effects (**Fig. 3B**), suggesting that the effect of talin1 KO on traction force may be caused by its suppression of cell spreading.

Since talin1 head domain (TH1) has been reported to mediate cell spreading in talin1-KO cells (Zhang et al., 2008), we examined whether transfection of TH1 could rescue the traction force production in talin1-null cells. Talin1-null U2 OS cells were transfected with EGFP-TH1 ($talin1_{1-446}$) and –TH2 ($talin2_{1-449}$), respectively (**Fig. 4A**). The cells were plated on polyacrylamide gels containing Red FluoSpheres for cell spreading and traction force assays, using talin1-KO cells as a control. Transfection of talin1-KO cells with TH1 significantly rescued the cell spreading defect, while transfection with TH2 had no effect (**Fig. 4B&C**). TH1-mediated cell spreading was accompanied by an increase in traction force, while TH2 was unable to rescue the cell spreading and traction force defect caused by talin1 ablation (**Fig. 4B&D**). Since the talin head domain lacks the major actin-binding site (Atherton et al., 2015), it is deficient in mediating traction force production. These results suggest that the apparent role of talin1 in traction force is partially caused by its effect on cell spreading.

To explore whether talin2 is dispensable in traction force generation, talin2-KO U2 OS cells were transfected with full-length (FL) pEGFP-talin1 or –talin2 (**Fig. 4E**) and the traction force in these cells were determined, using talin2-KO cells and CRISPR vector cells as controls. Transfection with talin1 caused only a slight increase in traction force, whereas transfection with talin2 almost restored the traction force to the levels of CRISPR control cells (**Fig. 4F**). The role of talin2 in traction force production is further supported by shRNA knockdown experiments, where depletion of talin2 caused significant reduction in traction force production in U2 OS cells and MDA-MB-231 cells (**Figure S3**). These results indicate that talin2 is indispensable for cellular traction force generation.

Strong binding of talin2 to integrins is essential for the development of traction force

To stably express full-length $talin2^{WT}$ and $talin2^{S339C}$ in talin2-null U2 OS cells, pAAVS1-EGFP-$talin2^{WT}$ or –$talin2^{S339C}$ were co-transfected with AAVS1 gRNA into talin2-null U2 OS cells. The cells were selected with neomycin and sorted for EGFP positive cells. The expression of EGFP-$talin2^{WT}$ and –$talin2^{S339C}$ was examined by Western blotting **(Fig. 5A)**. To

examine whether the strong binding of talin2 to β-integrins is essential for traction force generation, talin2-null cells that express EGFP-talin2^{WT} or –talin2^{S339C} were plated on the gelatin-conjugated polyacrylamide gels containing Red FluoSpheres, and traction force was measured using talin2-null cells and CRISPR vector cells as controls. Expression of EGFP-talin2^{WT} in talin2-null cells restored more than 70% of traction force, whereas that of EGFP-talin2^{S339C}, which has reduced affinity to β-integrins, had little effect (**Fig. 5B&C**). This result suggests that a strong binding of talin2 to β-integrins is required for traction force generation.

Strong binding of talin2 to integrins is required for cell invasion

To examine the role of talin1 and talin2 in cell invasion, talin1- or talin2-ablated U2 OS cells were examined for their capacities to penetrate through transwell filters coated with Matrigel. As shown in **Fig. 6A&B**, ablation of either talin1 or talin2 inhibited the invasion of U2 OS cells. Talin1 or talin2 KO caused approximately 77-91% inhibition of U2 OS cell invasion. This critical role of talin1 and talin2 in cell invasion was also observed in MDA-MB-231 cells (**Fig. 6C**). These results indicate that both talin1 and talin2 play critical roles in cell invasion.

To determine the essential role of the talin2-β-integrin interaction in cell invasion, talin2-null U2 OS cells that express EGFP-talin2^{WT} or –talin2^{S339C} were tested for their invasive capacities toward Matrigel, using talin2-null cells and CRISPR vector cells as controls. Expression of EGFP-talin2^{WT} in talin2-null cells significantly rescued the cell invasion, whereas that of EGFP-talin2^{S339C}, had only slight effect (**Fig. 6D&E**), suggesting that strong binding of talin2 to integrins is required for cell invasion.

Talin2 co-localizes with invadopodia and regulates matrix degradation

To examine the co-localization of talin2 with invadopodia, U2 OS cells were plated on Cy3-labeled gelatin that was immobilized on glass-bottom dishes, and co-stained for talin2 and a invadopodium marker, cortactin or Tks5. Talin2 significantly co-localized with cortactin and Tks5 at either large or small degradation holes (**Fig. 7A&B**). More than 80% of invadopodia co-localized with talin2. MDA-MB-231 cells had more robust invadopodia, where talin2 co-

localized with cortactin, as compared to U2 OS cells (**Fig. 7C**). Talin1 also co-localized with invadopodia in MDA-MB-231 cells (**Supplementary Fig. S4A**). We then examined the co-localization of talin2 with two other invadopodium markers, β1-integrin and N-WASP. The β1-integrin and talin2 co-localized with degradation holes in U2 OS cells, whereas β1-integrin at FAs did not (**Supplementary Fig. S4B**). Talin2 also co-localized with N-WASP at invadopodia-like structures (**Supplementary Fig. S4C**). These results suggest that talin2 is a marker for invadopodia.

To determine the roles of talin1 and talin2 in invadopodia, talin1 or talin2-ablated U2 OS cells were plated on Alexa488-labeled gelatin and stained for filamentous actin. Although ablation of either talin1 or talin2 dramatically inhibited invadopodium-mediated matrix degradation, talin2 KO had slightly more severe effect on invadopodia than talin1 KO (**Fig. 7D&E**), suggesting a key role of talin2 in invadopodium regulation.

To examine whether talin2 is indispensable for invadopodium-mediated matrix degradation, talin2-KO U2 OS cells were transfected with full-length pEGFP-talin1 or -talin2, and the matrix degradation in these cells were determined, using talin2-KO and CRISPR vector cells as controls. Transfection with talin1 did not significantly improve invadopodial matrix degradation, whereas transfection with talin2 rescued the invadopodia in talin2-KO cells (**Fig. 7F&G**). Using shRNA to deplete talin2 also caused significant reduction in invadopodium formation in U2 OS cells (**Figure S4E**). However, talin2 KO did not affect the invadopodium-like staining of cortactin (**Fig. S4D**). These results suggest that talin2 is indispensable for invadopodium-mediated matrix degradation.

Talin2-mediated traction force drives invadopodium-mediated matrix degradation

To learn whether the traction force distribution is co-localized with invadopodia, U2 OS cells were plated on Alexa488-gelatin-conjugated polyacrylamide gels containing Red FluoSpheres. Invadopodia and traction force were measured simultaneously using a Nikon A1 confocal microscope. As shown in **Fig. 8A&B**, traction force was co-localized with approximately 65% of

degraded holes of invadopodia, suggesting that traction force may regulate invadopodium-mediated matrix degradation.

To examine whether talin2-mediated traction force regulates invadopodium-mediated matrix degradation, talin2-null U2 OS cells that stably express EGFP-talin2^{WT} or –talin2^{S339C} were plated on glass-bottom dishes immobilized with Cy3-gelatin, using talin2-KO cells and CRISPR vector cells as controls. Talin2^{WT} formed invadopodium-like structures, whereas talin2^{S339C} was deficient to do so **(Fig. 8C&D)**. Expression of talin2^{WT} in talin2-null cells completely restored invadopodium-mediated matrix degradation, whereas expression of talin2^{S339C}, which is deficient in traction force, did not (**Fig. 8E**).

To test the role of talin2-mediated traction force in invadopodia in another cell line, talin2 in MDA-MB-231 cells was ablated by infecting the cells with lentiviruses that express Cas9 and talin2 gRNAs. AAVS1 gRNA were co-transfected with pAAVS1-EGFP-talin2^{WT} and pAAVS1-EGFP–talin2^{S339C,} respectively, into talin2-null cells. The expression of EGFP-talin2^{WT} and EGFP-talin2^{S339C} in talin2-null MDA-MB-231 cells was detected using an anti-talin2 antibody **(Fig. 8F)**. Similar to the results observed in U2 OS cells, talin2^{WT} markedly restored the invadopodia in talin2-null MDA-MB231 cells, whereas talin2^{S339C} had little effect **(Fig. 8G&H)**. Thus, talin2-mediated traction force might regulate invadopodium-mediated matrix degradation.

Discussion

In invasive cells, talin2 generates strong traction force through its high affinity to β-integrins, driving invadopodium-mediated matrix degradation and ultimately, cell invasion (**Fig. 8I**). Thus, talin2 binding to β-integrin tails is indispensable for cancer cell invasion.

We found that talin2 binds integrin tails stronger than talin1 does and that talin2 S339 contributes to its strong interaction with β-integrins. Substitution of S339 with Cys caused a reduction in its binding to integrins, whereas the reciprocal mutation of talin1 C336 to Ser enhanced talin1 binding (**Fig. 1**). Our data are different from the results of a previous report

(Anthis et al., 2009), where the F3 domains of talin1 and talin2 bound to β1A tails with Kd of 491 and 652 μM, respectively, as measured by NMR. In our study, we found that talin2 had a stronger interaction with β-integrin tails than talin1; this discrepancy is probably because we used the full-length talin2 head domain while the F3 domain alone was used in Anthis' experiments. Indeed, the talin2 head domain bound to β1A tails much more efficiently than the F2-F3 domain (**Fig. S1C**). This is consistent with a previous report (Calderwood et al., 1999). The discrepancy could be also caused by the different buffers used in the assays, where we included 3 mg/ml BSA or 0.5 mg/ml gelatin in our binding buffer to reduce non-specific binding. Our findings provide a molecular basis to explain the different roles of talin1 and talin2.

Talin1 and talin2 have distinct roles in regulating FA assembly. Based on FAK and Zyxin staining, talin1 knockout or knockdown inhibited small FAs (<7 μm^2), but had no effect on large FAs (>7 μm^2) (**Fig. 2; Fig. S2**). Talin2 knockout or knockdown also suppressed Zyxin localizing to FAs, but did not influence the recruitment of FAK to FAs. These results are consistent with previous findings obtained in talin-1 knockout cells (Zhang et al., 2008). Since Zyxin is a marker for FA maturation (Zaidel-Bar et al., 2003), these results suggest that talin1 regulates small FA assembly, whereas talin2 controls larger, more stable FA formation. Talin1-mediated smaller FAs may contribute to FA dynamics and cell migration (Huang et al., 2009), whereas the property of talin2 to aggregate into large assemblies may stabilize invadopodia.

We found that talin2 played an important role in traction force generation. Either talin2 KO or KD suppressed traction force generation (**Fig. 3; Fig. S3**). Moreover, the traction force in talin2-KO cells can be rescued by transfecting with talin2, but not with talin1, indicating the indispensable role of talin2 in traction force generation (**Fig. 4**). Furthermore, talin2-mediated traction force is dependent on its strong interaction with integrin tails (**Fig. 5**). Talin2-mediated traction force generation could be related to the role of talin2 in large FA formation, because FAs regulate traction force generation (Dumbauld et al., 2013; Hinz and Gabbiani, 2003;

Morimatsu et al., 2015). Ablation of talin1 caused a reduction in traction force, but this effect can be partially attributed to the role of talin1 in cell spreading (**Figs. 3 and 4**), because: 1) talin1 KO also inhibited cell spreading (**Fig. 3**); 2) expression of the talin1 head domain in talin1 null cells promoted spreading and traction force generation (**Fig. 4**). The talin1 head domain retains the integrin activation function of talin1, thus promoting cell spreading (Calderwood et al., 1999; Zhang et al., 2008). However, it lacks the major actin binding site and is deficient in mediating traction force (Zhang et al., 2008). The distinct roles of talin1 and talin2 in cell spreading and traction force could be caused by their different binding affinities toward β-integrins. This assertion is supported by the deficiency of talin2^{S339C} in mediating traction force (**Fig. 5**). It is possible that the different mechanical properties between talin1 and talin2 rod domains may contribute to traction force generation (Austen et al., 2015). Taken together, it is likely that talin1 indirectly modulates traction force through promoting cell spreading, whereas talin2 may directly control traction force by acting as a mechanical transmitter between integrins and the actin cytoskeleton.

Although it has been reported that talin2 is not essential for fibroblast migration (Debrand et al., 2012) , we demonstrate that it plays an important role in cell invasion. Either talin2 KO or KD inhibited cancer cell invasion **(Fig. 6)**. Furthermore, re-expression of talin2^{WT} in talin2-null cells rescued cell invasion, whereas re-expression of talin2^{S339C}, which is deficient in β integrin-binding, did not (**Fig. 6**). The role of talin2 in cell invasion can be attributed to its effect on invadopodium-mediated matrix degradation, a key regulatory point for cell invasion (Beaty and Condeelis, 2014; Bergman et al., 2014; Paz et al., 2014; Weaver, 2006; Yamaguchi et al., 2006).

Invadopodia are large assemblies that mediate cell invasion (Beaty and Condeelis, 2014; Paz et al., 2014; Revach and Geiger, 2013). We found that talin2 considerably co-localized with invadopodia (**Fig. 7**). In fact, large and round talin2 staining spots usually co-localized with invadopodia. Ablation of either talin1 or talin2 reduced invadopodium-mediated matrix

degradation, but ablation of talin2 had slightly more effects than that of talin1 (**Fig. 7**). Furthermore, expression of full-length talin2^{WT} rescued invadopodium-mediated matrix degradation in talin2-null cells, whereas expression of talin2^{S339C}, which has reduced binding to β1-integrin tails, had little effect (**Fig. 8**). These results suggest that a strong interaction between talin2 and β-integrin tails is indispensable for invadopodium-mediated matrix degradation.

Interestingly, regions of high traction forces also co-localized with invadopodia (**Fig. 8A**). Re-expression of talin2^{WT} but not talin2^{S339C} in talin2-null cells restored the traction force generation and invadopodium-mediated matrix degradation (**Fig. 5; Fig. 8**). These results suggest that binding of talin2 to β-integrin tails is essential for the generation of traction force, which in turn drives invadopodium-mediated matrix degradation and cancer cell invasion.

It has been reported that podosomes, similar structures to invadopodia, develop in the absence of traction force (Yu et al., 2013). We found here that talin2-mediated traction force was required for invadopodium-mediated matrix degradation. However, talin2 seems not to be required for the initial development of invadopodia, because talin2 KO did not influence the assembly of cortactin, an invadopodium marker, into invadopodium-like structures (**Fig. S4**). Thus, talin2-mediated traction force may instead regulate invadopodium stability or maturation. Although we still do not understand how traction force regulates invadopodia, our findings fill in the gaps of our existing knowledge of talin2 and uncover novel but fundamental roles of talin2 in mediating traction force and invadopodium development during cell invasion.

Talin1 is generally thought to play more important roles in cell migration and embryogenesis: talin1 knockout causes embryonic lethality in mice (Monkley et al., 2000), whereas talin2 is not essential for mouse embryonic development (Debrand et al., 2012). However, as we show here, talin2 generates traction force to mediate invadopodium formation and cell invasion. The recent identification of a human pathology arising from a missense variant, S339L, of the Tln2 gene resulting in the digit deformity, fifth finger camptodactyly (Deng et al., 2016), demonstrates

the physiological importance of S339 in talin2 function and the requirement for a robust talin2:integrin linkage for normal development. Both an S339C and the disease copying S339L mutant reduced the affinity of talin2 for integrin and the ability of cells to generate traction forces. It is possible that the deleterious effect of this mutation on integrin binding and traction force generation may be the cause of the developmental abnormality. Interestingly, talin2 was found to be down-regulated by trastuzumab, a HER2-targeting antibody drug for breast cancers (Le et al., 2012). Thus, inhibition of talin2 function could be a potential strategy for cancer therapy.

Materials and methods

Reagents

Anti-talin1 (clone 97H6) and anti-talin2 (clone 53.8) antibodies were from AbD Serotec. Anti-zyxin (clone EPR4302) rabbit monoclonal antibody was from Abcam. Anti-cortactin mouse monoclonal antibody (clone 4F11) and anti-Tks5 rabbit polyclonal antibody (SH3 #4) were from EMD Millipore. Anti-cortactin (H222) rabbit polyclonal and anti-N-WASP (clone 30D10) rabbit monoclonal antibodies were from Cell Signaling Technology. Anti-β1-integrin monoclonal antibody (P5D2) was from R&D Systems. Anti-FAK[pY397] (clone 18/FAK (pY397)) was from BD Biosciences. Anti-talin2 (GW22654) chicken polyclonal and anti-tubulin (clone B-5-1-2) monoclonal antibodies bovine skin gelatin and pLKO1 lentivirus shRNAs that respectively target talin1 and talin2 were from Sigma. Talin1 shRNA clones are TRCN0000123105 (#1), TRCN0000299020 (#2). Talin2 shRNA clones are TRCN0000122990 (#1) and TRCN0000122992 (#2). LentiCRISPRv2 and pSpCas9(BB)-2A-Puro V2.0, which were generated by Feng Zhang's Lab (Ran et al., 2013), were from Addgene. Alexa488-labeled gelatin and Red FluoSpheres were from Life Technologies. Cy3 dye was from Click Chemistry Tools. Gelatin was labeled with Cy3 according to the manufacturer's instruction. DyLight 488 conjugated goat anti-mouse IgG (H+L) and Alexa Fluor 488 labeled goat anti-chicken IgY (H+L)

were from Thermo Scientific. Dylight 550 or 633 labeled goat anti-mouse and anti-rabbit IgG (H+L) were from Immunoreagents (Raleigh, NC). anti-Fibronectin and recombinant human EGF were from Akron Biotech; Growth factor reduced Matrigel was from BD Bioscience. Pfu Ultra was from Agilent Technologies. Cold Fusion Cloning Kit was from System Biosciences (Palo Alto, CA). Anti-GFP monoclonal antibody and Safectine RU50 transfection kit were purchased from Syd Labs (Malden, MA). DNA primers were synthesized by Integrated DNA Technologies.

Plasmid construction

The full-length pEGFP-talin2 WT was subcloned by the following steps: 1) DNA fragments encoding residues 1-1159 of human talin2 were amplified by Pfu Ultra-based PCR using human talin2 cDNA clone as template and 5'-atg cac tcg agc tat ggt ggc cct gtc ctt aaa gat ttgt-3' / 5'-act gag gta ccg tct cga gca gaa tct aac atg gca t-3' as primers and subcloned into pEGFP-C1 via Xho1/Kpn1 sites; 2) fragments encoding residues 1160-2543 of talin2 were amplified using human cDNA from U2 OS cells and 5'-ggc tgc atc gac aac cga ccc c-3'/5'-tat tat cta gat tag ccc tca tct tcc ctc agc tc-3' and subcloned into the resulted plasmid in step 1 via Not1/Xba1 sites. pEGFP-talin2$_{1\text{-}449}$ was generated by amplifying DNA fragments encoding residues 1-449 using 5'-atg cac tcg agc tat ggt ggc cct gtc ctt aaa gat ttg t-3' / 5'-ggg ccc gtc gac tat gag ccg tgc tct gcc ttc cc-3' as primers and subcloning into pEGFP-C1 vector via Xho1/Sal1 sites. pEGFP-talin1$_{1\text{-}446}$ was generated by amplifying DNA fragments encoding residues 1-446 using 5'-ggg ccc gaa ttc tat ggt tgc act ttc act gaa gat cag-3' / 5'-ggg ccc gtc gac tta aga gcc atg ctc cac ttt ccc c-3' as primers and subcloning into pEGFP-C1 vector via EcoR1/Sal1 sites. pEGFP-talin2$_{1\text{-}449}^{S339C}$ was created by pfu Ultra-based PCR using pEGFP-talin2$_{1\text{-}449}$ as template and 5'-gga tca cca aag act gtg tga tgc gcg tgg-3' / 5'-cca cgc gca tca cac agt ctt tgg tga tcc-3' as primers. pEGFP-talin1$_{1\text{-}446}^{C336S}$ was created by PCR using pEGFP-talin1$_{1\text{-}446}$ as template and 5'-cat cac caa gga gag tgt gat gcg ag-3' / 5'- ctc gca tca cac tct cct tgg tga tg -3' as primers. pEGFP-talin1$_{1\text{-}433}$ was reported previously (Huang et al., 2009). pQE-talin1$_{1\text{-}446}$ and -talin2$_{1\text{-}449}$ were generated by amplifying the DNA fragments using 5'-ggg ccc gag ctc atg gtt gca ctt tca ctg aag

atc ag-3'/5'-ggg ccc gtc gac tta aga gcc atg ctc cac ttt ccc c-3' and 5'-atg cag aat cca tgg tgg ccc tgt cct taa aga ttt gt-3'/5'-ggg ccc gtc gac tat gag ccg tgc tct gcc ttc cc-3' as primers and subcloning into pQE-30 vector via Sac1/Sal1 and BamH1/Sal1, respectively. The rescue plasmids pEGFP-talin2$_{1\text{-}449}$-R and pEGFP-talin2$_{1\text{-}449}^{S339C}$-R were created by PCR using pEGFP-talin2$_{1\text{-}449}$ as template and 5'-gtg aag acc atg cag ttc gag cca tct aca gct gt-3' / 5'-aca gct gta gat ggc tcg aac tgc atg gtc ttc ac-3' as primers. The full-length rescue plasmids pEGFP-talin2-R and pEGFP-talin2^{S339C}-R were created by digesting full-length pEGFP-talin2 with BsrG1/EcoRV and ligating the resulting larger fragment with the smaller fragments from the rescue plasmids pEGFP-talin2$_{1\text{-}449}$-R and pEGFP-talin2$_{1\text{-}449}^{S339C}$-R. The full-length pAAVS1-EGFP-talin2 and pAAVS1-EGFP-talin2^{S339C} were created by subcloning talin2 and the mutant into pAAVS1-EGFP vector, using the same strategy as used to subclone full-length pEGFP-talin2. The pAAVS1-EGFP vector was generated by the following procedures: 1)pEGFP-C1 with BsiWI (at nt 20) and AscI (at nt 3533) was created by sequential PCR using pEGFP-C1 as template and 5'-gtt att aat agt aat cac gta cgg ggt cat tag ttc ata g-3' / 5'-cta tga act aat gac ccc gta cgt gat tac tat taa taa c-3' and 5'-cgg aat cgt ttt ccg gcg cgc cgg ctg gat gat c-3' / 5'-gat cat cca gcc ggc gcg ccg gaa aac gat tcc g-3' as primers; 2) the left and right homologous arms of AAVS1 were amplified by PCR using 5'-tta ata gta atc acg tac gtg ctt tct ctg acc agc att c-3' / 5'-atg aac taa tga ccc cgt acg gcc cca ctg tgg ggt gga-3' and 5'-cgg aat cgt ttt ccg gcg cgc cac tag gga cag gat tgg tg-3' / 5'-gga tca tcc agc cgg cgc gcc aga gca gag cca gga acc c-3' as primers, and subcloned into the modified pEGFP-C1 vector via BsiWI and AscI, respectively, using the Cold Fusion Cloning Kit. AAVS1 gRNA was generated by annealing oligos 5'-cac cgc tag tgg ccc cac tgt ggg g-3' / 5'-aaa ccc cca cag tgg ggc cac tag c-3' and subcloning into BbsI–digested pSpCas9(BB)-2A-Puro V2.0 vector. LentiCRISPR-TLN1 was created by annealing oligos 5'-cac cgg gat ccg ctc acg aat gat g-3' / 5'-aaa cca tca ttc gtg agc gga tcc c-3' and subcloning into BsmB1-digested lentiCRISPRv2 vector. LentiCRISPR-TLN2 was generated by annealing oligos 5'-cac cgc gtg tcg agt cat tcg gga a-3' / 5'-aaa ctt ccc gaa tga ctc gac acg c-3' and subcloning

into lentiCRISPRv2 vector. All plasmids were sequenced by Eurofins MWG Operon (Huntsville, AL).

Cell culture and transfection CHO-K1 Chinese hamster ovary cells, MDA-MB-231 human breast cancer cells, U2 OS human bone osteosarcoma cells and 293T human embryonic kidney cells were from the American Type Culture Collection and were maintained in DMEM medium (Corning Inc.) containing 10% fetal bovine serum (FBS), penicillin (100 U/ml) and streptomycin (100 µg/ml). CHO-K1 and 293T cells were transfected with Safectine RU50 according to the manufacturer's protocol. U2 OS cells were transfected with Mirus Ingenio solution using GenePulser Xcell (Bio-Rad Inc., Hercules, CA).

Tln1 and Tln2 KO by CRISPR Preparation of viruses and cell infection were performed as described previously (Li et al., 2013; Wu et al., 2011). LentiCRISPR-TLN1 and lentiCRISPR-TLN2 were co-transfected with packaging vectors pMDLg/pRRE, pRSV-Rev and CMV-VSVG into 293FT cells. Lentiviral particles were collected and used to infect U2 OS cells. The cells were selected with puromycin and clones isolated. Tln1 or Tln2 KO clones were detected by Western blotting using anti-talin1 and anti-talin2 monoclonal antibodies.

Re-expression of talin2 and talin2^{S339C} in talin2 null cells The AAVS1 gRNA was co-transfected with pAAVS1-EGFP-talin2^{WT} and -EGFP-talin2^{S339C}, into talin2 null cells. Transfected cells were selected with neomycin. EGFP-positive cells were sorted by flow cytometry, or EGFP-positive clones were isolated.

Protein interaction assays CHO-K1 cells were transfected with pEGFP-talin1$_{1-433}$, -talin1$_{1-446}$, -talin1$_{1-449}$, or their mutants. At 28 h post-transfection, the cells were harvested in lysis buffer A (50 mM Tris-HCl pH 7.4, 1% NP‑40, 150 mM NaCl, 1 mM EDTA and a protease inhibitor cocktail). Cell lysates were cleared by centrifugation and incubated with glutathione–Sepharose beads loaded with GST or GST-β-integrin tails at 4 ℃ for 2 h. The beads were washed with the lysis buffer 4 times and resuspended in SDS-sample buffer. Samples were analyzed using

SDS–PAGE and transferred to nitrocellulose membrane for the detection of interacting proteins. The binding of purified His-tagged proteins to GST-β-integrin tails was performed in lysis Buffer A containing 3 mg/ml BSA (Fig. 1D) or 0.5 mg/ml gelatin (Fig. 1I).

Cell invasion assays Cell invasion was performed as described previously (Li et al., 2013). Briefly, 100 µl of Matrigel (1:30 dilution in serum-free DMEM medium) was added to each Transwell polycarbonate filter and incubated at 37 ℃ for 5 h. Cells were trypsinized and washed 3 times with DMEM containing 1% FBS. The cells were resuspended in DMEM containing 1% FBS at a density of 5×10^5 cells/ml. The cell suspensions (100 µl) were seeded into the upper chambers, and 600 µl of DMEM medium containing 1% FBS, 20 ng/ml EGF and 10 µg/ml fibronectin were added to the lower chambers. The cells were allowed to invade for 12 h (or as indicated) in a CO2 incubator, fixed, stained and quantitated as described previously (Wu et al., 2011).

Traction force measurement Glass-bottom dishes were silanized by 0.5% silane, and activated by 0.5% glutaraldehyde. A drop of gel solution containing acrylamide (6%), bis-acrylamide (0.75%), ammonium persulfate (APS), TEMED, and FluoSpheres® carboxylate-modified beads (diameter 0.2 µm, 1:85 dilution by volume) was added to the dishes and covered by a coverslip. The coverslip was removed, and gels were activated with sulfo-SANPAH under UVA exposure and then conjugated with gelatin (0.2 mg/ml). Cells were plated on the gels and traction force was measured as described previously (Butler et al., 2002), using an A1 confocal microscope in Lexington VA Medical Center.

Invadopodium assays Glass-bottom dishes were coated with 100 µl of warm Alexa488-conjugated gelatin (0.2 mg/ml) in PBS containing 2% sucrose. The coated dishes were dried, fixed with pre-chilled glutaraldehyde solution (0.5% in PBS), washed with PBS and then reduced with 5 mg/ml of sodium borohydride in PBS. The dishes were washed extensively with PBS and then incubated with DMEM containing 10% FBS and antibiotics for 1h. Cells were plated at low density to the dishes and cultured for 24h, fixed with paraformaldehyde and

stained for talin2 (or talin1) and F-actin. Images were acquired using a TIRF microscope. To measure invadopodium areas, the images were converted to 16 bit inverted JPEG format (invadopodia are white spots) using ImageJ. The images were then opened with NIS Elements, thresholded (invadopodium spots were precisely covered by red). A Region-Of-Interests (ROIs) was drawn along the cell edge and the total invadopodium area was measured using NIS Elements.

Competing interests

The authors declare no competing or financial interests.

Acknowledgements

We thank Dr. Berni Wehrle-Haller for his participation in the project discussion; Dr. Ken Jacobson (UNC-Chapel Hill) for the technique of traction force assays; Latifeh Azizi (U. Tampere) for her support in affinity assays; Drs. Berni Wehrle-Haller, Ken Jacobson and Andrew Morris for critical reading of this manuscript. This work was supported by a start-up fund from Markey Cancer Center, University of Kentucky and American Cancer Society IRG 85-001-22 and Research Scholar Grant RSG-13-184-01CSM (to CH) and BBSRC Project Grant BB/N007336/1 to (BG).

Author contributions L.Q., N.J., X.L. and L.L. performed experiments, analyzed data, and wrote the paper; Z.C. instructed the traction force measurement and analysis; V.P. and B.T.G helped with affinity assays and manuscript writing; C.-G.Z. performed computational analysis; C.H. designed experiments, interpreted results and wrote the paper.

References

Anthis, N.J., Wegener, K.L., Ye, F., Kim, C., Goult, B.T., Lowe, E.D., Vakonakis, I., Bate, N., Critchley, D.R., Ginsberg, M.H., et al. (2009). The structure of an integrin/talin complex reveals the basis of inside-out signal transduction. *EMBO J.* **28**:3623-3632.

Atherton, P., Stutchbury, B., Wang, D.-Y., Jethwa, D., Tsang, R., Meiler-Rodriguez, E., Wang, P., Bate, N., Zent, R., Barsukov, I.L., et al. (2015). Vinculin controls talin engagement with the actomyosin machinery. *Nat. Commun*. **6**.

Austen, K., Ringer, P., Mehlich, A., Chrostek-Grashoff, A., Kluger, C., Klingner, C., Sabass, B., Zent, R., Rief, M., and Grashoff, C. (2015). Extracellular rigidity sensing by talin isoform-specific mechanical linkages. *Nat. Cell Biol*. **17**:1597-1606.

Bate, N., Gingras, A.R., Bachir, A., Horwitz, R., Ye, F., Patel, B., Goult, B.T., and Critchley, D.R. (2012). Talin Contains A C-Terminal Calpain2 Cleavage Site Important In Focal Adhesion Dynamics. *PLoS ONE* **7**:e34461.

Beaty, B.T., and Condeelis, J. (2014). Digging a little deeper: The stages of invadopodium formation and maturation. *Eur. J. Cell Biol*. **93**:438-444.

Beaty, B.T., Wang, Y., Bravo-Cordero, J.J., Sharma, V.P., Miskolci, V., Hodgson, L., and Condeelis, J. (2014). Talin regulates moesin–NHE-1 recruitment to invadopodia and promotes mammary tumor metastasis. *J. Cell Biol*. **205**:737-751.

Bergman, A., Condeelis, J.S., and Gligorijevic, B. (2014). Invadopodia in context. *Cell Adh. Migr*. **8**:273-279.

Butler, J.P., Tolić-Nørrelykke, I.M., Fabry, B., and Fredberg, J.J. (2002). Traction fields, moments, and strain energy that cells exert on their surroundings. *Am. J. Physiol. Cell Physiol*. **282**:C595-C605.

Calderwood, D.A., Zent, R., Grant, R., Rees, D.J.G., Hynes, R.O., and Ginsberg, M.H. (1999). The Talin Head Domain Binds to Integrin β Subunit Cytoplasmic Tails and Regulates Integrin Activation. *J. Biol. Chem*. **274**:28071-28074.

Chen, C., Wang, X., Xiong, X., Liu, Q., Huang, Y., Xu, Q., Hu, J., Ge, G., and Ling, K. (2015). Targeting type I[gamma] phosphatidylinositol phosphate kinase inhibits breast cancer metastasis. *Oncogene* **34**:4635-4646.

Debrand, E., Conti, F.J., Bate, N., Spence, L., Mazzeo, D., Pritchard, C.A., Monkley, S.J., and Critchley, D.R. (2012). Mice carrying a complete deletion of the talin2 coding sequence are viable and fertile. *Biochem. Biophys. Res. Commun*. **426**:190-195.

Deng, H., Deng, S., Xu, H., Deng, H.-X., Chen, Y., Yuan, L., Deng, X., Yang, S., Guan, L., Zhang, J., et al. (2016). Exome Sequencing of a Pedigree Reveals S339L Mutation in the *TLN2* Gene as a Cause of Fifth Finger Camptodactyly. *PLoS ONE* **11**:e0155180.

Desiniotis, A., and Kyprianou, N. (2011). Chapter four - Significance of Talin in Cancer Progression and Metastasis. *Int. Rev. Cell Mol. Biol*. **289**:117-147.

Di Paolo, G., Pellegrini, L., Letinic, K., Cestra, G., Zoncu, R., Voronov, S., Chang, S., Guo, J., Wenk, M.R., and De Camilli, P. (2002). Recruitment and regulation of phosphatidylinositol phosphate kinase type 1[gamma] by the FERM domain of talin. *Nature*. **420**:85-89.

Franco, S.J., Rodgers, M.A., Perrin, B.J., Han, J., Bennin, D.A., Critchley, D.R., and Huttenlocher, A. (2004). Calpain-mediated proteolysis of talin regulates adhesion dynamics. *Nat Cell Biol*. **6**:977-983.

Giannone, G., Jiang, G., Sutton, D.H., Critchley, D.R., and Sheetz, M.P. (2003). Talin1 is critical for force-dependent reinforcement of initial integrin–cytoskeleton bonds but not tyrosine kinase activation. *J. Cell Biol*. **163**:409-419.

Gingras, A.R., Ziegler, W.H., Frank, R., Barsukov, I.L., Roberts, G.C.K., Critchley, D.R., and Emsley, J. (2005). Mapping and Consensus Sequence Identification for Multiple Vinculin Binding Sites within the Talin Rod. *J. Biol. Chem*. **280**:37217-37224.

Goult, B.T., Zacharchenko, T., Bate, N., Tsang, R., Hey, F., Gingras, A.R., Elliott, P.R., Roberts, G.C.K., Ballestrem, C., Critchley, D.R., et al. (2013). RIAM and Vinculin Binding to Talin Are Mutually Exclusive and Regulate Adhesion Assembly and Turnover. *J. Biol. Chem*. **288**:8238-8249.

Hemmings, L., Rees, D.J., Ohanian, V., Bolton, S.J., Gilmore, A.P., Patel, B., Priddle, H., Trevithick, J.E., Hynes, R.O., and Critchley, D.R. (1996). Talin contains three actin-binding sites each of which is adjacent to a vinculin-binding site. *J. Cell Sci*. **109**:2715-2726.

Huang, C., Rajfur, Z., Yousefi, N., Chen, Z., Jacobson, K., and Ginsberg, M.H. (2009). Talin phosphorylation by Cdk5 regulates Smurf1-mediated talin head ubiquitylation and cell migration. *Nat. Cell Biol*. **11**:624-630.

Jin, J.K., Tien, P.C., Cheng, C.J., Song, J.H., Huang, C., Lin, S.H., and Gallick, G.E. (2015). Talin1 phosphorylation activates [beta]1 integrins: a novel mechanism to promote prostate cancer bone metastasis. *Oncogene*. **34**:1811-1821.

Le, X.-F., Almeida, M.I., Mao, W., Spizzo, R., Rossi, S., Nicoloso, M.S., Zhang, S., Wu, Y., Calin, G.A., and Bast, R.C., Jr. (2012). Modulation of MicroRNA-194 and Cell Migration by HER2-Targeting Trastuzumab in Breast Cancer. *PLoS ONE* **7**:e41170.

Li, X., Zhou, Q., Sunkara, M., Kutys, M.L., Wu, Z., Rychahou, P., Morris, A.J., Zhu, H., Evers, B.M., and Huang, C. (2013). Ubiquitylation of phosphatidylinositol 4-phosphate 5-kinase type I γ by HECTD1 regulates focal adhesion dynamics and cell migration. *J. Cell Sci*. **126**:2617-2628.

Ling, K., Doughman, R.L., Firestone, A.J., Bunce, M.W., and Anderson, R.A. (2002). Type I[gamma] phosphatidylinositol phosphate kinase targets and regulates focal adhesions. *Nature*. **420**:89-93.

Monkley, S.J., Zhou, X.-H., Kinston, S.J., Giblett, S.M., Hemmings, L., Priddle, H., Brown, J.E., Pritchard, C.A., Critchley, D.R., and Fässler, R. (2000). Disruption of the talin gene arrests mouse development at the gastrulation stage. *Dev. Dyn*. **219**:560-574.

Nayal, A., Webb, D.J., and Horwitz, A.F. (2004). Talin: an emerging focal point of adhesion dynamics. *Curr. Opin. Cell Biol*. **16**:94-98.

Nuckolls, G.H., Turner, C.E., and Burridge, K. (1990). FUNCTIONAL-STUDIES OF THE DOMAINS OF TALIN. *J. Cell Biol*. **110**:1635-1644.

Paz, H., Pathak, N., and Yang, J. (2014). Invading one step at a time: the role of invadopodia in tumor metastasis. *Oncogene*. **33**:4193-4202.

Praekelt, U., Kopp, P.M., Rehm, K., Linder, S., Bate, N., Patel, B., Debrand, E., Manso, A.M., Ross, R.S., Conti, F., et al. (2012). New isoform-specific monoclonal antibodies reveal different sub-cellular localisations for talin1 and talin2. *Eur. J. Cell Biol*. **91**:180-191.

Ran, F.A., Hsu, P.D., Wright, J., Agarwala, V., Scott, D.A., and Zhang, F. (2013). Genome engineering using the CRISPR-Cas9 system. *Nat. Protocols*. **8**:2281-2308.

Revach, O.-Y., and Geiger, B. (2013). The interplay between the proteolytic, invasive, and adhesive domains of invadopodia and their roles in cancer invasion. *Cell Adh. Migr*. **8**:215-225.

Saykali, B.A., and El-Sibai, M. (2014). Invadopodia, Regulation, and Assembly in Cancer Cell Invasion. *Cell Commun. Adhes*. **21**:207-212.

Senetar, M.A., Moncman, C.L., and McCann, R.O. (2007). Talin2 is induced during striated muscle differentiation and is targeted to stable adhesion complexes in mature muscle. *Cell Motil. Cytoskeleton*. **64**:157-173.

Tadokoro, S., Shattil, S.J., Eto, K., Tai, V., Liddington, R.C., de Pereda, J.M., Ginsberg, M.H., and Calderwood, D.A. (2003). Talin Binding to Integrin ß Tails: A Final Common Step in Integrin Activation. *Science* **302**:103-106.

Weaver, A. (2006). Invadopodia: Specialized Cell Structures for Cancer Invasion. *Clin. Exp. Metastasis* **23**:97-105.

Webb, D.J., Parsons, J.T., and Horwitz, A.F. (2002). Adhesion assembly, disassembly and turnover in migrating cells - over and over and over again. *Nat. Cell Biol*. **4**:E97-E100.

Wehrle-Haller, B. (2012). Assembly and disassembly of cell matrix adhesions. *Curr. Opin. Cell Biol*. **24**:569-581.

Wu, Z., Li, X., Sunkara, M., Spearman, H., Morris, A.J., and Huang, C. (2011). PIPKIγ Regulates Focal Adhesion Dynamics and Colon Cancer Cell Invasion. *PLoS ONE* **6**:e24775.

Yamaguchi, H., Pixley, F., and Condeelis, J. (2006). Invadopodia and podosomes in tumor invasion. *Eur. J. Cell Biol*. **85**:213-218.

Yu, C.-h., Rafiq, Nisha Bte M., Krishnasamy, A., Hartman, Kevin L., Jones, Gareth E., Bershadsky, Alexander D., and Sheetz, Michael P. (2013). Integrin-Matrix Clusters Form Podosome-like Adhesions in the Absence of Traction Forces. *Cell Reports* **5**:1456-1468.

Zaidel-Bar, R., Ballestrem, C., Kam, Z., and Geiger, B. (2003). Early molecular events in the assembly of matrix adhesions at the leading edge of migrating cells. *J. Cell Sci*. **116**:4605-4613.

Zhang, X., Jiang, G., Cai, Y., Monkley, S.J., Critchley, D.R., and Sheetz, M.P. (2008). Talin depletion reveals independence of initial cell spreading from integrin activation and traction. *Nat. Cell Biol*. **10**:1062-1068.

Figure legends

Figure 1. Talin2 has a much higher affinity to β-integrin tails than talin1. A-C. Binding of talin truncated mutants to β1A-integrin tails measured by GST pull-down assays. The EGFP fusion proteins of talin mutants were transiently expressed in CHO-K1 cells. **A.** Binding of EGFP-talin1_{1-433}, -talin1_{1-446}, and -talin2_{1-449}. **B.** Binding of EGFP-talin1_{1-446}, -talin2_{1-449}, -talin2_{1-}

$_{403}$ and –talin2$_{389-449}$. **C.** Binding of EGFP-talin1$_{1-446}$, -talin1$_{1-401}$, -talin1$_{395-446}$ and -talin2$_{1-449}$. **D.** Interaction of purified His-tagged-talin1$_{1-446}$ and -talin2$_{1-449}$ to immobilized GST and GST-β1A tails. The binding was detected by Coomassie staining. **E.** Sequence alignment of the integrin-binding region of the F3 domains of talin1 and talin2. C336 in talin1 and S339 in talin2 are shown in red. **F-H.** The EGFP fusion proteins of talin mutants were transiently expressed in CHO-K1 cells. The binding of talin mutants to β1A-integrin tails was determined by GST-pull-down assays. **F.** Substitution of talin1 C336 with Ser promoted its binding to β1A-integrin tails. **G.** Substitution of talin2 S339 with Cys reduced its binding to β1A integrin tails. **H.** Substitution of talin2 S339 with Leu diminished its binding to β1A integrin tails. **I.** Binding of purified His-tagged-talin1$_{1-446}$, -talin1$_{1-446}^{C336S,}$ -talin2$_{1-449}$, and talin2$_{1-449}^{S339C}$ to immobilized GST and GST-β1A tails. Binding was detected by Coomassie staining.

Figure. 2. Talin1 is required for small FA formation, whereas talin2 is responsible for large, stable FA assembly. **A.** Endogenous talin1 and talin2 in CRISPR vector-transfected U2 OS cells and talin1 or talin2-null U2 OS cells. **B.** The distribution of Zyxin and talin1 (top) or talin2 (bottom) in talin1- or talin2-null cells. Talin1 or talin2-null U2 OS cells were plated on fibronectin (5 μg/ml)-coated glass-bottom dishes for 4 h, fixed and co-stained for talin1 (or talin2) and Zyxin. Images were acquired by TIRF microscopy. Scale bar, 20 μm. **C.** Area distribution of Zyxin staining in talin1- (top) and talin2- (middle)-null U2 OS cells. The small graph in the bottom highlights the different effects of talin1 or talin2 KO on large (>10 μm^2) FAs. Data are mean ± SEM of 3 experiments. In each experiment, FAs of 20 cells from each group were analyzed and plotted. *t*-test, *P<0.05, **P<0.01, ***P < 0.001. **D.** Area distribution of talin1 and talin2 staining in central parts (5 μm from edges) of cells. Data are mean ± SEM of 3 experiments. *t*-test, *P<0.05. **E.** The distribution of FAK[pY397] in talin1- or talin2-null cells. Talin1 or talin2-null U2 OS cells were cultured on fibronectin, fixed and stained for FAK[pY397]. Scale bar, 20 μm. **F.** Area distribution of FAK[pY397] staining in talin1- (left) and talin2- (right)-

null U2 OS cells. Data are mean of 2 experiments. In each experiment, FAs of 20 cells from each group were analyzed and plotted.

Figure 3. The roles of talin1 and talin2 in cell spreading and traction force production. A. Effects of talin1 and talin2 KO on cell spreading and traction force generation in U2 OS cells. Scale bar, 30 μm. **B.** Quantitative cell spreading area in talin1- or talin2-ablated U2 OS cells, using cells carrying CRISPR vector as a control. Data are presented as mean ± SEM of 3 experiments. In each experiment, 30 cells from each group were analyzed. *t*-test, *P < 0.05, ***P < 0.001. **C.** Quantitative constrained traction force in talin1- or talin2-ablated U2 OS cells, using cells carrying CRISPR vector as a control. Data are presented as mean ± SEM of 3 independent experiments. *t*-test, ***P < 0.001.

Figure 4. Talin2 is indispensable for traction force generation. **A**. Expression of EGFP-talin1 head domain (TH1) and -talin2 head domain (TH2) in talin1-KO U2 OS cells. **B-D.** Expression of TH1 but not TH2 partially rescued the cell spreading and traction force defect caused by talin1-KO. **B.** Talin1-KO U2OS cells were transiently transfected with EGFP-TH1 or TH2, and cultured on polyacrylamide gel containing Red FluoSpheres for determining the cell spreading and traction force, using CRISPR vector-infected cells and talin1-KO cells as controls. Scale bar, 30 μm. **C.** Quantitative cell spreading areas on polyacrylamide gel. Data are presented as mean ± SEM of 3 experiments. In each experiment, 30 cells from each group were analyzed. *t*-test, **P<0.01. **D.** Quantitative constrained traction force. Data are presented as mean ± SEM of 3 independent experiments. In each experiment, more than 30 cells from each group were analyzed. *t*-test, **P<0.01. **E.** Transient expression of full-length EGFP-talin1 and -talin2 in talin2-KO U2 OS cells. **F.** Re-expression of full-length EGFP-talin2 rescued the traction force defect caused by talin2 KO, whereas re-expression of talin1 only induced slight increase in traction force. Data are presented as mean ± SEM of 4 experiments. In each experiment, more than 40 cells from each group were analyzed. *t*-test,*P<0.05, ***P<0.001.

Figure 5. Strong binding of talin2 to β-integrin tails is required for traction force generation. **A.** Stable expression of EGFP-talin2^{WT} and -talin2^{S339C} in talin2-null U2 OS cells using CRISPR. **B-C.** Re-expression of talin2^{WT} in talin2-null cells restored their traction force generation, but that of talin2^{S339C} did not. **B.** Talin2-null U2 OS cells that express EGFP-talin2^{WT} or –talin2^{S339C} were cultured on polyacrylamide gel containing Red FluoSpheres for determining traction force, using CRISPR vector-infected cells and talin2-null cells as controls. Scale bar, 30 μm. **C.** Quantitative constrained traction force. Data are presented as mean ± SEM of 3 experiments. In each experiment, more than 30 cells from each group were analyzed. *t*-test, *P<0.05, **P<0.01.

Figure 6. Strong binding of talin2 to integrins is required for cell invasion. **A.** Ablation of either talin1 or talin2 inhibited the invasion of U2 OS cells. **B.** Quantification of Experiment "A". Data are presented as mean ± SEM from 3 independent experiments. *t*-test, *P<0.05, **P<0.01. **C.** Depletion of either talin1 or talin2 using shRNAs inhibited the invasion of MDA-MB-231 cells. Data are presented as mean ± SEM from 3 independent experiments. *t*-test, **P<0.01, ***P<0.001. **D.** Talin2-null U2 OS cells that express EGFP-talin2^{WT} or –talin2^{S339C} were examined for their Matrigel invasive capacities, using CRISPR vector-infected cells and talin2-null cells as controls. **E.** Quantification of Experiment "D". Data are presented as mean ± SEM from 3 independent experiments. *t*-test, *P<0.05.

Figure 7. Talin2 is indispensable for invadopodium-mediated matrix degradation. **A, B.** Talin2 co-localized with cortactin (A) and Tks5 (B) at invadopodia in U2 OS cells plated on Cy3–labeled gelatin for 16 h. Cells were co-stained with a chicken anti-talin2 and a rabbit anti-cortactin antibodies (A), or with an anti-talin2 and an anti-Tks5 (B) antibodies. Representative TIRF images are showed. Arrowheads point to mature invadopodia with co-localization of talin2 and cortactin (A) or Tks5 (B). Insets show magnified small invadopodia in the box. Scale Bars: 20 μm. Graphs show the mean degradation spots with cortactin (left bar) and with both cortactin and talin2 (right bar) (A), or with Tks5 (left bar) and with both Tks5 and talin2 (right bar)

(B). Data are presented as mean ± SEM of 40 cells from 2 independent experiments. **C.** Talin2 co-localized with cortactin at invadopodia in MDA-MB-231 cells plated on Cy3–labeled gelatin for 10 h. Scale Bars: 20 μm. **D.** Ablation of either talin1 or talin2 inhibited invadopodium-mediated matrix degradation. Talin1- or talin2-null U2 OS cells were cultured on Alexa488-gelatin immobilized on glass-bottom dishes, fixed and stained with Alexa647-phalloidin. Scale bar, 20 μm. **E.** Quantification of Experiment "D". Data are presented as mean ± SEM of 3 independent experiments. In each experiment, 20 cells from each group were analyzed. *t*-test, *P < 0.05, **P<0.01. **F.** Re-expression of full-length EGFP-talin2, but not -talin1, restored invadopodial matrix degradation in talin2-null cells. Talin2-KO U2 OS cells were transiently transfected with full-length EGFP-talin1 or -talin2, and cultured on Cy3-gelatin immobilized on glass-bottom dishes, fixed and stained with Alexa647-phalloidin, using CRISPR vector-infected cells and talin2-KO cells as controls. Scale bar, 20 μm. **G.** Quantification of the invadopodia in experiment "F". Data are presented as mean ± SEM of 3 independent experiments. *t*-test, *P<0.05.

Figure 8. Strong binding of talin2 to β-integrin tails is indispensable for invadopodium-mediated matrix degradation. **A.** The distribution of traction force was co-localized with invadopodia. US OS Cells were cultured on Alexa488-gelatin immobilized on acrylamide gel containing Red FluoSpheres. Traction force and invadopodium formation were determined using an A1 confocal microscope. Scale bar, 30 μm. **B.** Quantification of the co-localization of traction force and invadopodia. The gelatin degradation images were merged with traction force maps, and co-localization was examined manually. Data are presented as mean ± SEM of 24 cells from 3 independent experiments. **C-E.** Stable expression of EGFP-talin2^{WT} in talin2-null U2 OS cells restored invadopodial matrix degradation, but that of EGFP-talin2^{S339C} did not. **C.** Talin2-null U2 OS cells that stably express EGFP-talin2^{WT} or –talin2^{S339C} were cultured on Cy3-gelatin immobilized on glass-bottom dishes, fixed and stained for talin2. Scale bar, 20 μm. **D.** Quantitation of the assembly of talin2^{WT} and talin2S339C to invadopodium-like structures. Data

are presented as mean ± SEM of 3 independent experiments. **E.** Quantitation of invadopodium area. Data are presented as mean ± SEM of 3 independent experiments. In each experiment, 20 cells from each group were analyzed. *t*-test, *P<0.05, **P<0.01. **F-H.** Talin2-null MDA-MB-231 cells that express EGFP-talin2^{WT} or –talin2^{S339C} were cultured on Alexa Fluor 488-gelatin immobilized on glass-bottom dishes, fixed and stained with cortactin, using CRISPR vector-infected cells and talin2-KO cells as controls. **F.** Stable expression of EGFP-talin2^{WT} and -talin2^{S339C} in talin2-null MDA-MB-231 cells using CRISPR. **G.** Merged TIRF images of matrix degradation and cortactin staining. Scale bar, 20 µm. **H.** Expression of EGFP-talin2^{WT} in talin2-null MDA-MB-231 cells restored invadopodial matrix degradation, but that of EGFP-talin2^{S339C} did not. Data are presented as mean ± SEM of 3 independent experiments. *t*-test, *P<0.05, **P<0.01, ***P<0.001. **I.** A Proposed mechanism whereby talin2 regulates traction force generation, invadopodium-mediated matrix degradation and cancer cell invasion.

Qi et al. Figure 1

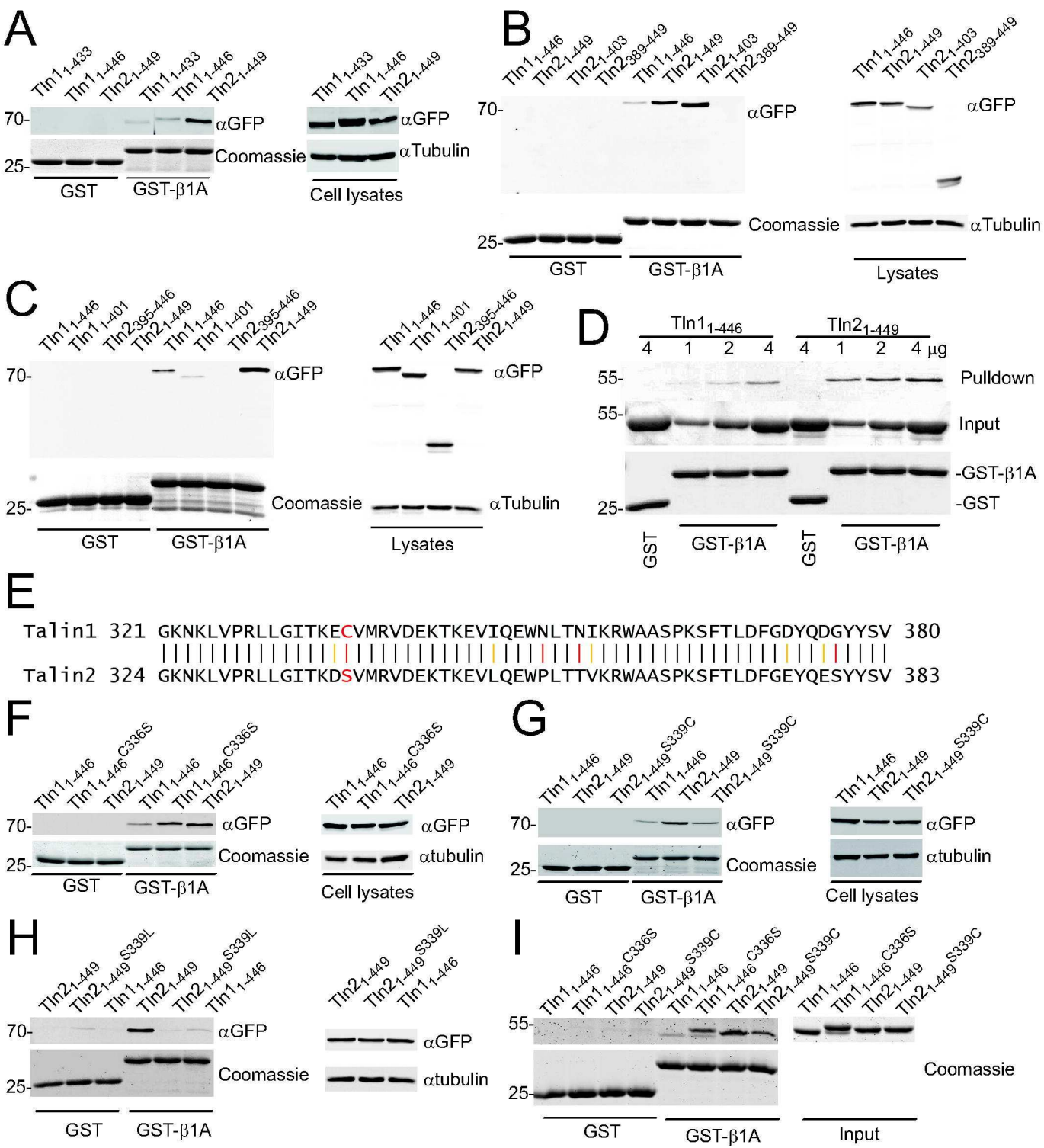

Qi et al Figure 2

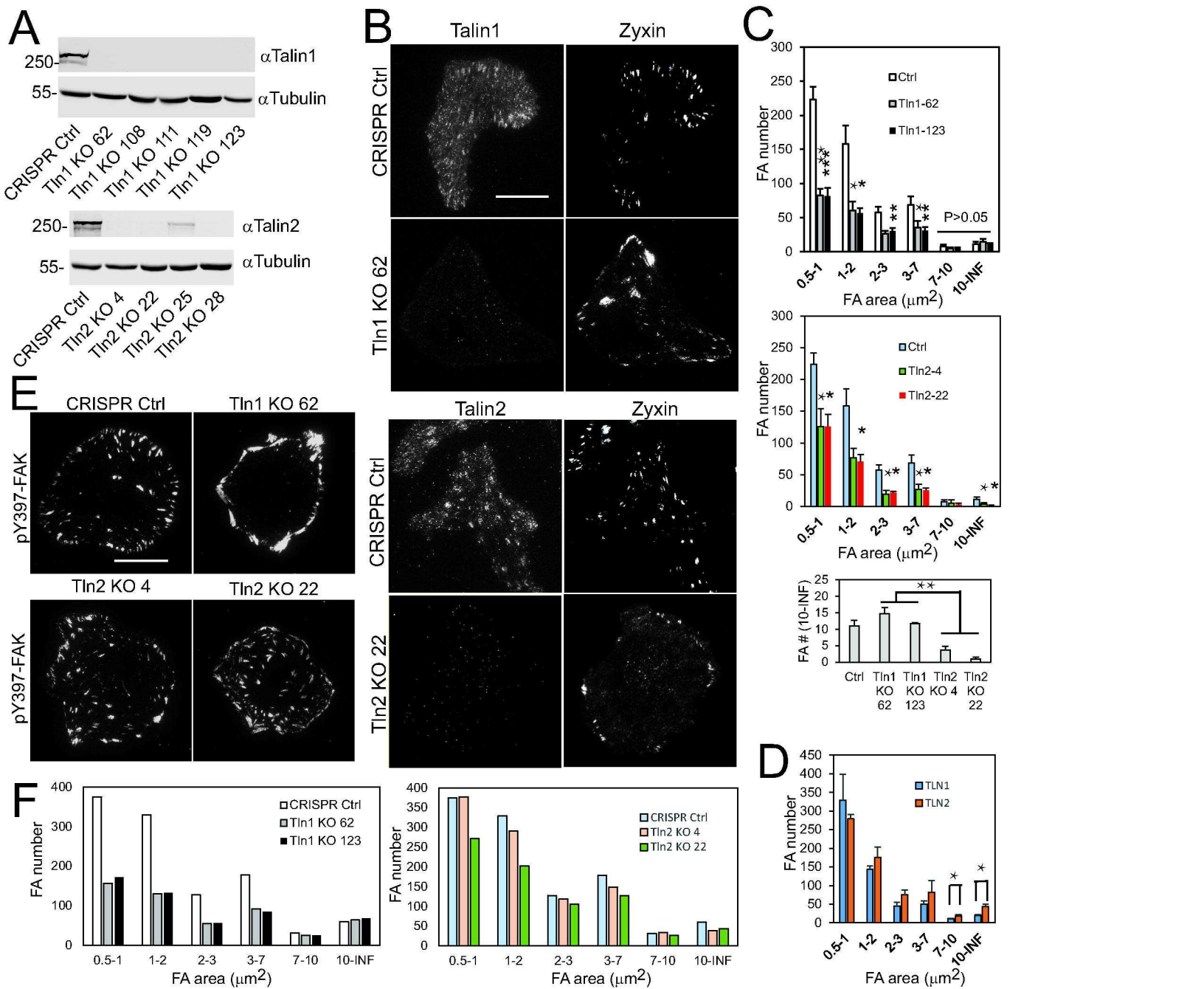

Qi et al. Fig. 3

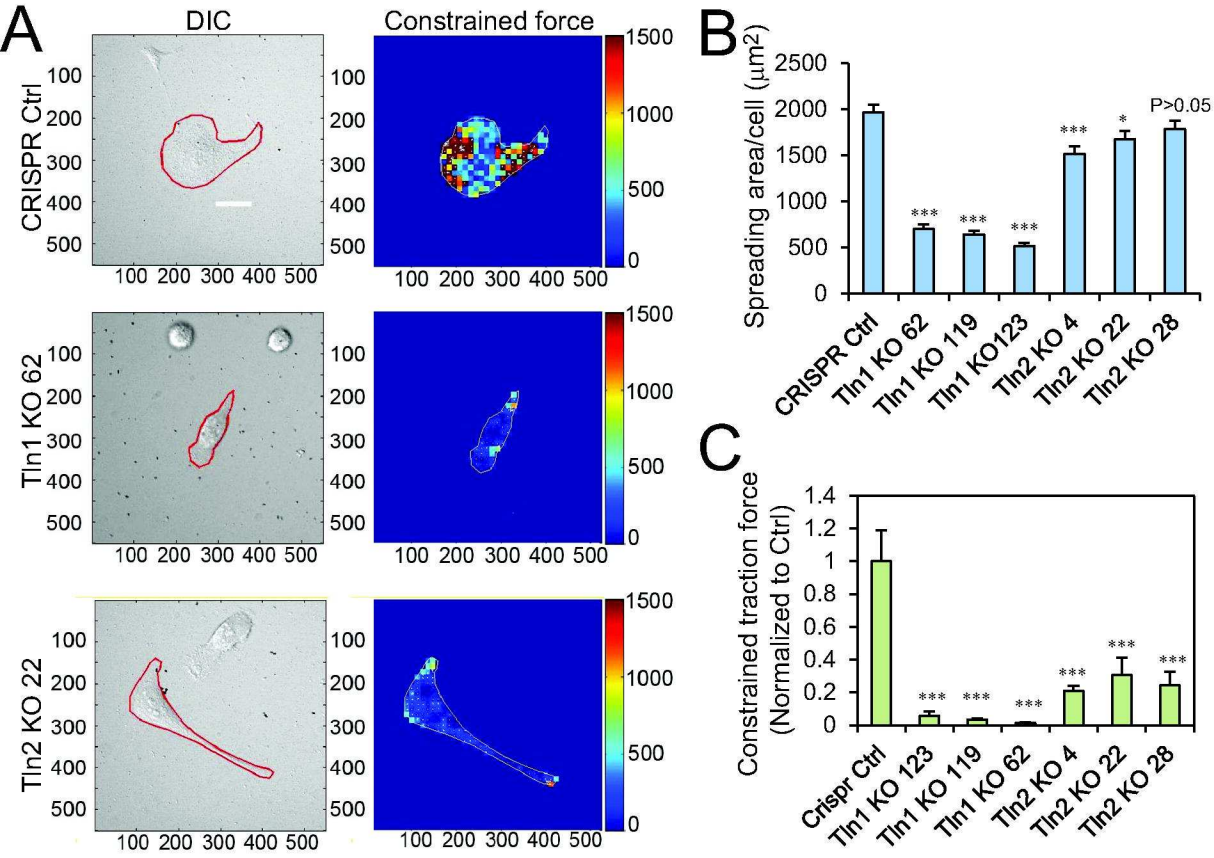
A
DIC
Constrained force
CRISPR Ctrl
Tln1 KO 62
Tln2 KO 22
100 200 300 400 500
1500
1000
500
0
B
Spreading area/cell (μm2)
2500
2000
1500
1000
500
0
***
*
P>0.05
CRISPR Ctrl
Tln1 KO 62
Tln1 KO 119
Tln1 KO123
Tln2 KO 4
Tln2 KO 22
Tln2 KO 28
C
Constrained traction force
(Normalized to Ctrl)
1.4
1.2
1
0.8
0.6
0.4
0.2
0
Crispr Ctrl
Tln1 KO 123
Tln1 KO 119
Tln1 KO 62
Tln2 KO 4
Tln2 KO 22
Tln2 KO 28

Qi et al. Fig. 4

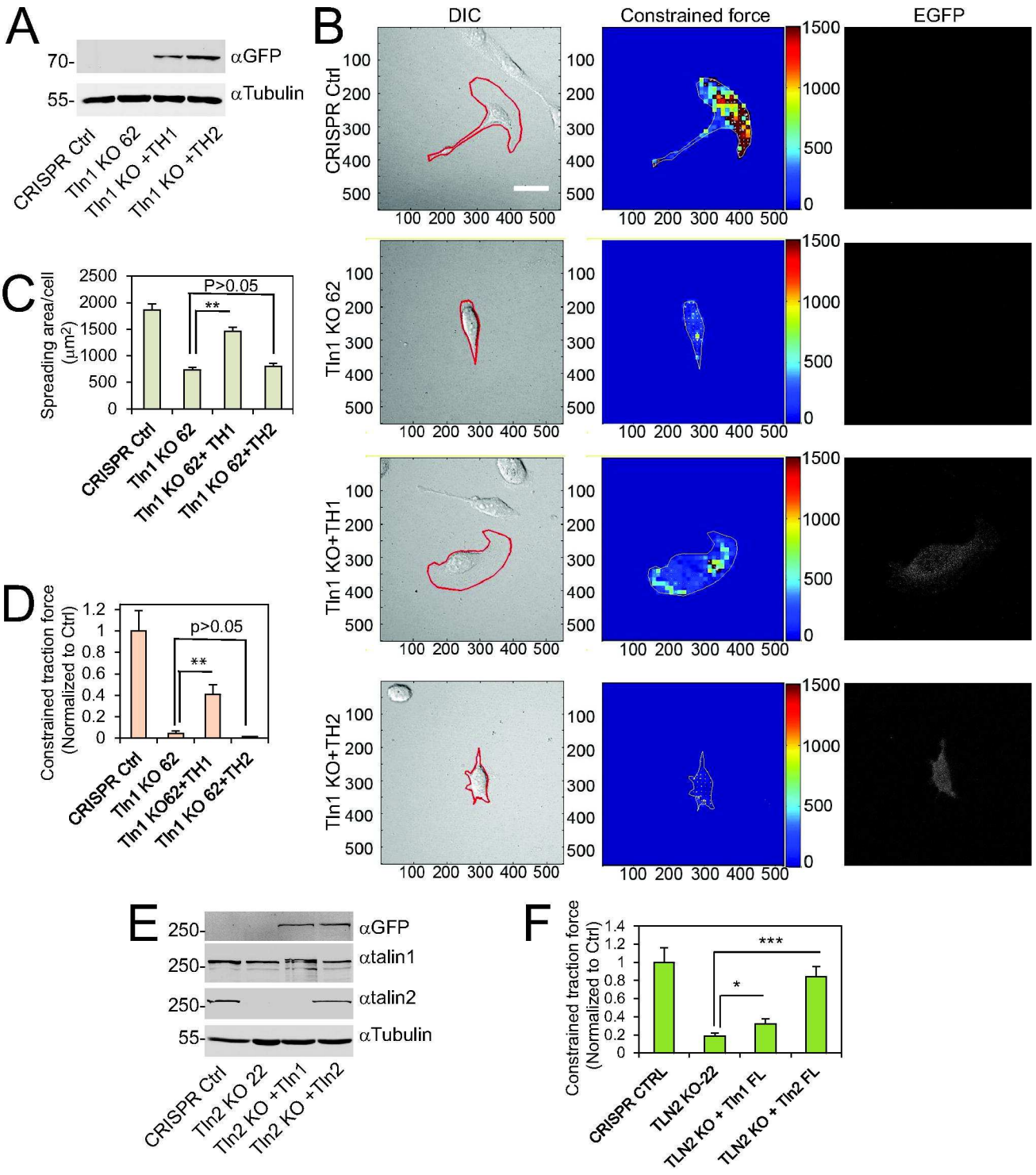
A
70-
αGFP
55-
αTubulin
CRISPR Ctrl
Tln1 KO 62
Tln1 KO +TH1
Tln1 KO +TH2
B
DIC
Constrained force
EGFP
CRISPR Ctrl
Tln1 KO 62
Tln1 KO+TH1
Tln1 KO+TH2
C
Spreading area/cell (μm2)
P>0.05
**
CRISPR Ctrl
Tln1 KO 62
Tln1 KO 62+ TH1
Tln1 KO 62+TH2
D
Constrained traction force (Normalized to Ctrl)
p>0.05
**
CRISPR Ctrl
Tln1 KO 62
Tln1 KO62+TH1
Tln1 KO 62+TH2
E
250-
αGFP
250-
αtalin1
250-
αtalin2
55-
αTubulin
CRISPR Ctrl
Tln2 KO 22
Tln2 KO +Tln1
Tln2 KO +Tln2
F
Constrained traction force (Normalized to Ctrl)
***
*
CRISPR CTRL
TLN2 KO-22
TLN2 KO + Tln1 FL
TLN2 KO + Tln2 FL

Qi et al Figure 5

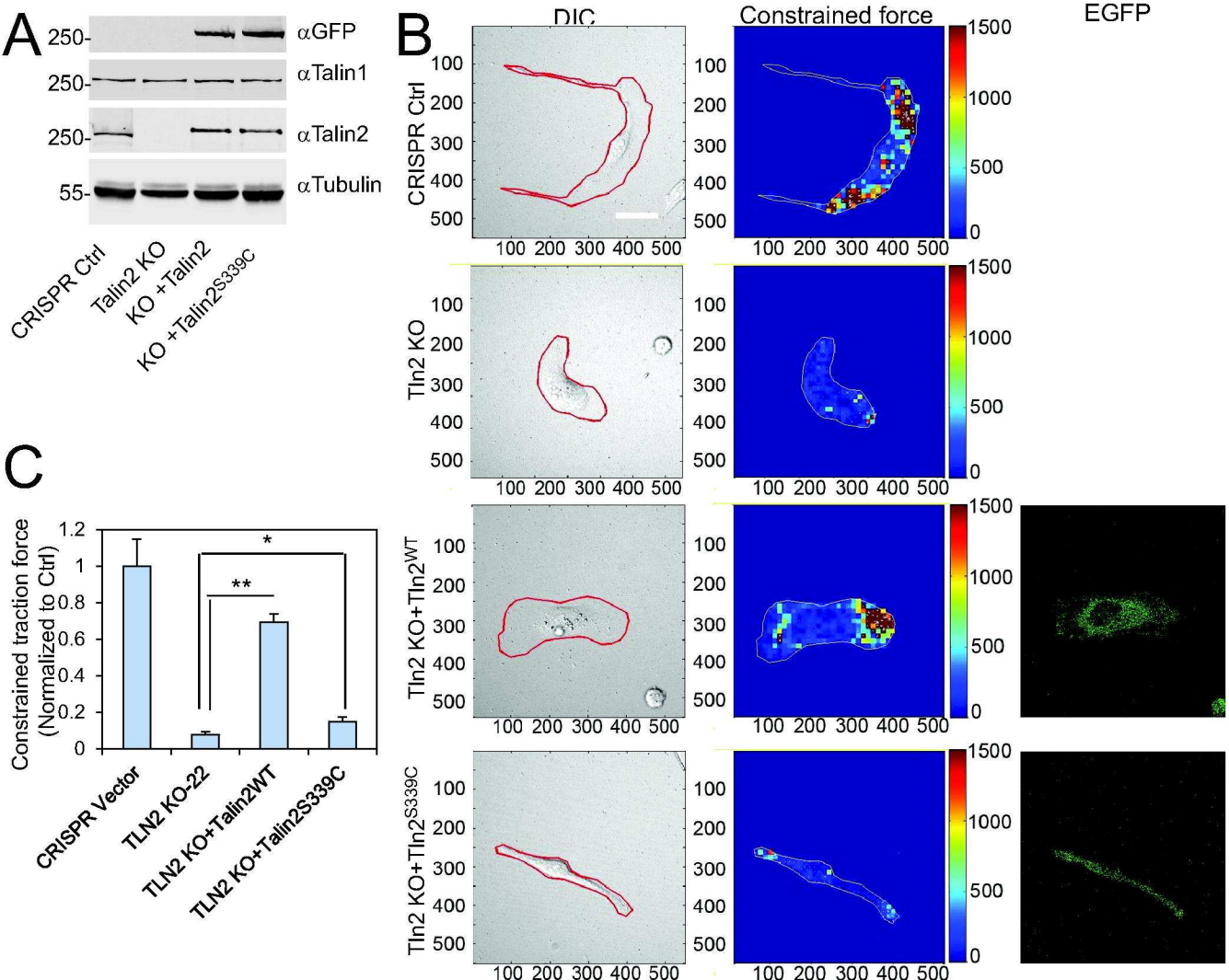

Qi et al. Fig. 6

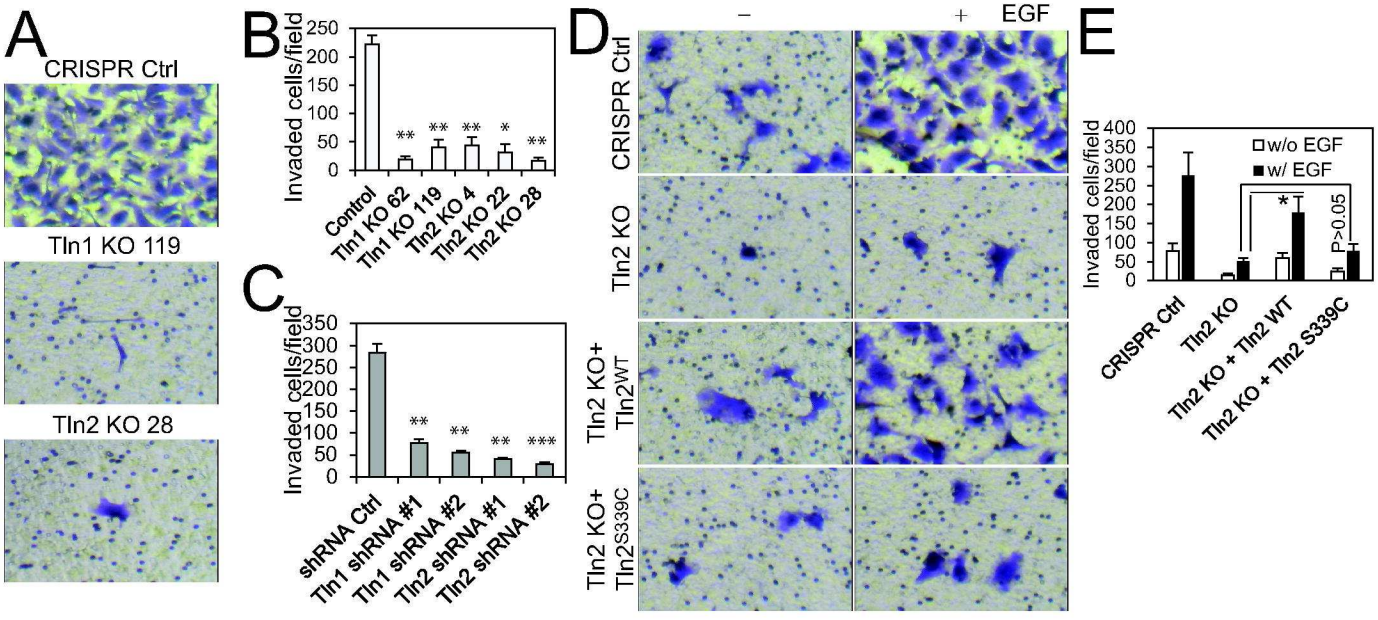
A
CRISPR Ctrl
Tln1 KO 119
Tln2 KO 28
B
Invaded cells/field
250
200
150
100
50
0
**
**
**
*
**
Control
Tln1 KO 62
Tln1 KO 119
Tln2 KO 4
Tln2 KO 22
Tln2 KO 28
C
Invaded cells/field
350
300
250
200
150
100
50
0
**
**
**
***
shRNA Ctrl
Tln1 shRNA #1
Tln1 shRNA #2
Tln2 shRNA #1
Tln2 shRNA #2
D
–
+
EGF
CRISPR Ctrl
Tln2 KO
Tln2 KO+ Tln2WT
Tln2 KO+ Tln2S339C
E
Invaded cells/field
400
350
300
250
200
150
100
50
0
w/o EGF
w/ EGF
*
P>0.05
CRISPR Ctrl
Tln2 KO
Tln2 KO + Tln2 WT
Tln2 KO + Tln2 S339C

Qi et al Figure 7

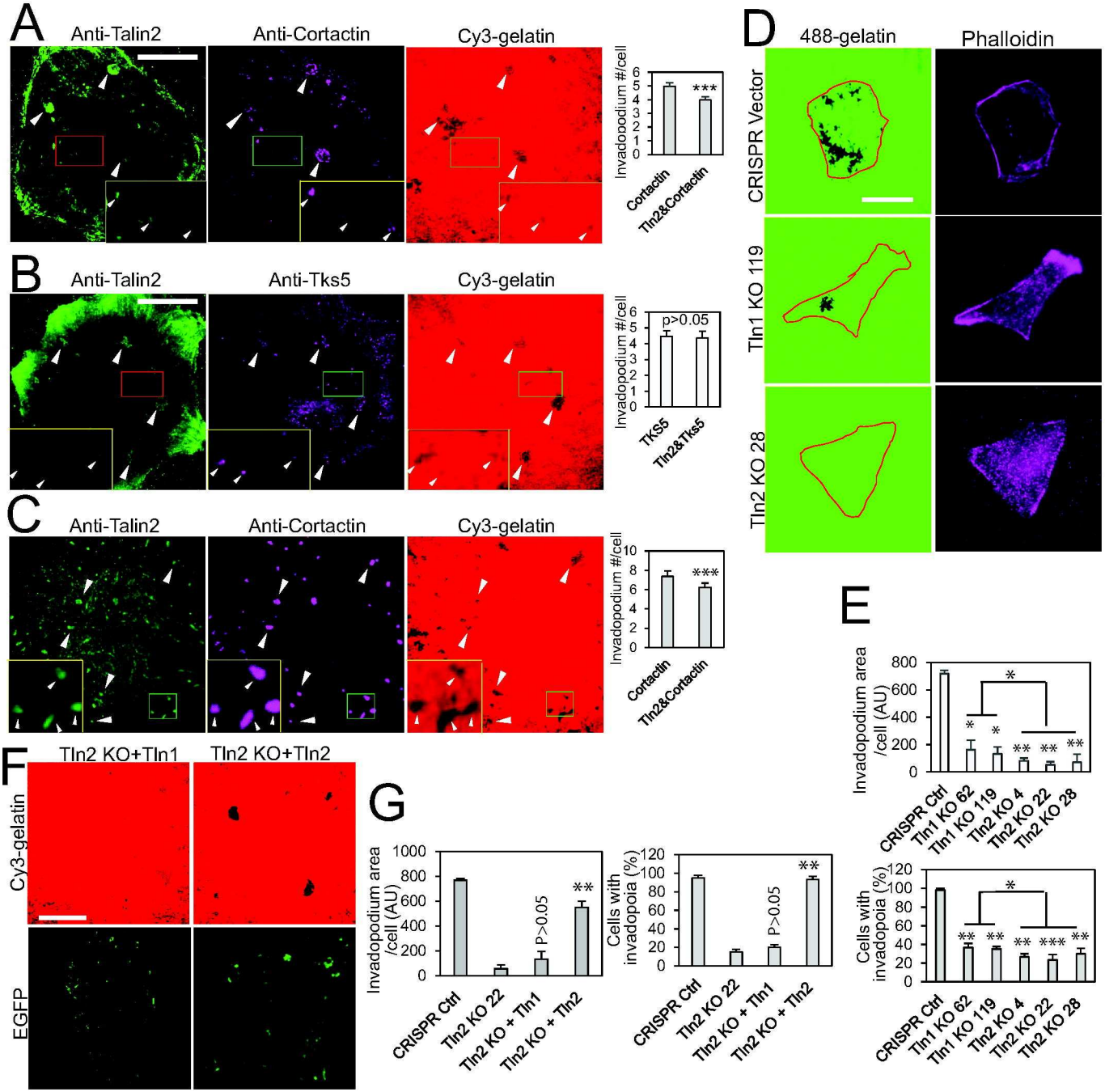

Qi et al Fig. 8

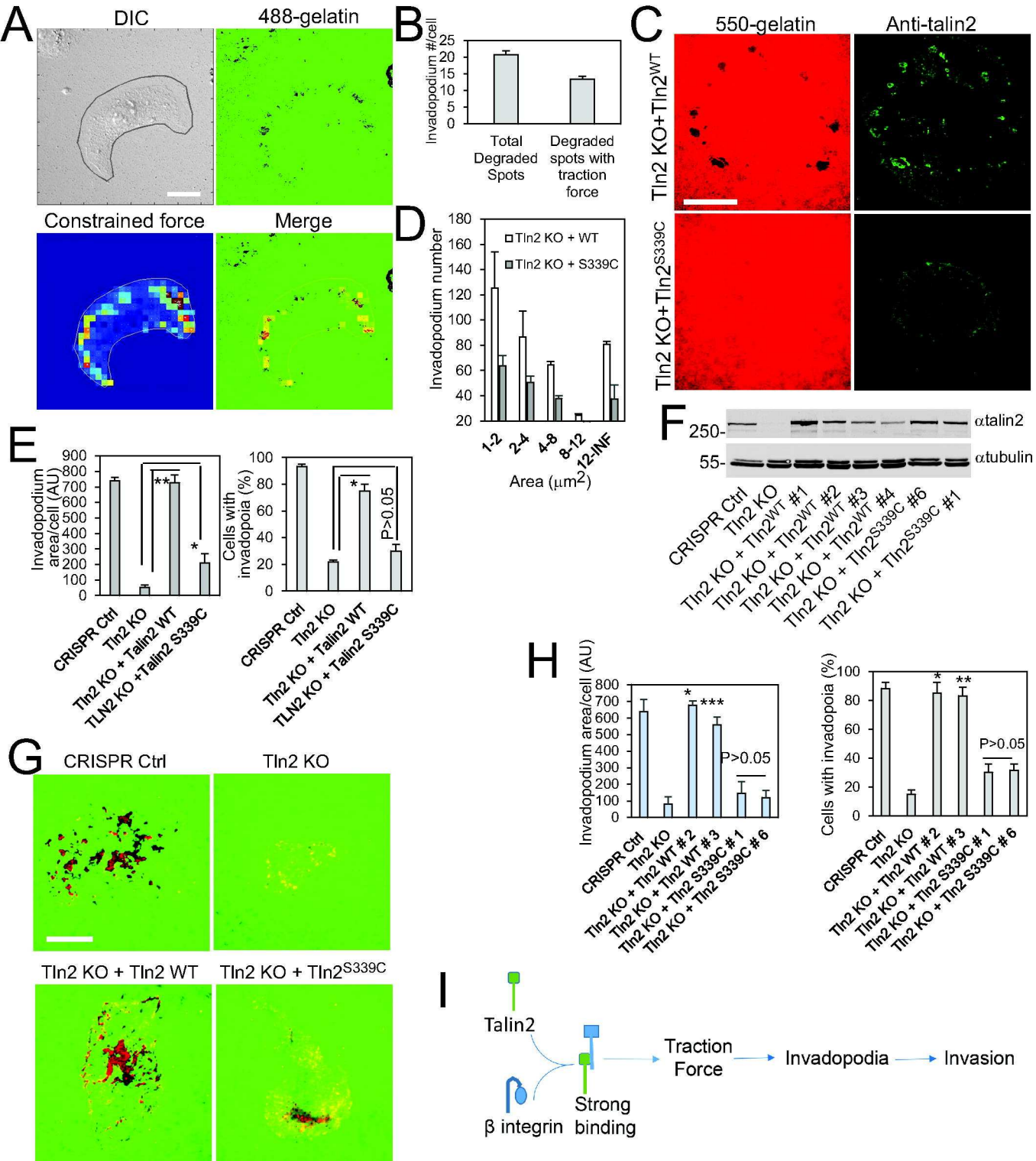
A
DIC
488-gelatin
Constrained force
Merge
B
Invadopodium #/cell
Total Degraded Spots
Degraded spots with traction force
C
550-gelatin
Anti-talin2
Tln2 KO+Tln2WT
Tln2 KO+Tln2S339C
D
Tln2 KO + WT
Tln2 KO + S339C
Invadopodium number
Area (μm2)
E
Invadopodium area/cell (AU)
Cells with invadopoia (%)
P>0.05
CRISPR Ctrl
Tln2 KO
Tln2 KO + Talin2 WT
TLN2 KO +Talin2 S339C
F
250-
55-
αtalin2
αtubulin
CRISPR Ctrl
Tln2 KO
Tln2 KO + Tln2WT #1
Tln2 KO + Tln2WT #2
Tln2 KO + Tln2WT #3
Tln2 KO + Tln2WT #4
Tln2 KO + Tln2S339C #6
Tln2 KO + Tln2S339C #1
G
CRISPR Ctrl
Tln2 KO
Tln2 KO + Tln2 WT
Tln2 KO + Tln2S339C
H
Invadopodium area/cell (AU)
Cells with invadopoia (%)
P>0.05
CRISPR Ctrl
Tln2 KO
Tln2 KO + Tln2 WT #2
Tln2 KO + Tln2 WT #3
Tln2 KO + Tln2 S339C #1
Tln2 KO + Tln2 S339C #6
I
Talin2
β integrin
Strong binding
Traction Force
Invadopodia
Invasion